2015

Photophoretictrapping-Raman spectroscopy for single pollens and fungal spores trapped in air

Chuji Wang
U.S. Army Research Laboratory, Adelphi, MD

Yong-Le Pan
U.S. Army Research Laboratory, Adelphi, MD

Steven C. Hill
U.S. Army Research Laboratory, Adelphi, MD

Brandon Redding
U.S. Army Research Laboratory, Adelphi, MD

Journal of Quantitative Spectroscopy & Radiative Transfer 153 (2015) 4–12

Contents lists available at ScienceDirect

Journal of Quantitative Spectroscopy & Radiative Transfer

journal homepage: www.elsevier.com/locate/jqsrt

Photophoretic trapping-Raman spectroscopy for single pollens and fungal spores trapped in air

Chuji Wang [a,b], Yong-Le Pan [a,*], Steven C. Hill [a], Brandon Redding [a]

[a] U.S. Army Research Laboratory, 2800 Powder Mill Road, Adelphi, MD 20783, USA
[b] Mississippi State University, Starkville, MS 39759, USA

ARTICLE INFO

Article history:
Received 30 April 2014
Received in revised form
4 November 2014
Accepted 6 November 2014
Available online 15 November 2014

Keywords:
Optical trapping
Raman spectroscopy
Bioaerosols
Pollen
Fungal spores
Single particle trapped in air

ABSTRACT

Photophoretic trapping-Raman spectroscopy (PTRS) is a new technique for measuring Raman spectra of particles that are held in air using photophoretic forces. It was initially demonstrated with Raman spectra of strongly-absorbing carbon nanoparticles (Pan et al. [44] (Opt Express 2012)). In the present paper we report the first demonstration of the use of PTRS to measure Raman spectra of absorbing and weakly-absorbing bioaerosol particles (pollens and spores). Raman spectra of three pollens and one smut spore in a size range of 6.2–41.8 μm illuminated at 488 nm are shown. Quality spectra were obtained in the Raman shift range of 1600–3400 cm^{-1} in this exploratory study. Distinguishable Raman scattering signals with one or a few clear Raman peaks for all four aerosol particles were observed within the wavenumber region 2940–3030 cm^{-1}. Peaks in this region are consistent with previous reports of Raman peaks in the 1600–3400 cm^{-1} range for pollens and spores excited at 514 nm measured by a conventional Raman spectrometer. Noise in the spectra, the fluorescence background, and the weak Raman signals in most of the 1600–3400 cm^{-1} region make some of the spectral features barely discernable or not discernable for these bioaerosols except the strong signal within 2940–3030 cm^{-1}. Up to five bands are identified in the three pollens and only two bands appear in the fungal spore, but this may be because the fungal spore is so much smaller than any of the pollens. The fungal spore signal relative to the air-nitrogen Raman band is approximately 10 times smaller than that ratio for the pollens. The five bands are tentatively assigned to the CH_2 symmetric stretch at 2948 cm^{-1}, CH_2 Fermi resonance stretch at 2970 cm^{-1}, CH_3 symmetric stretch at 2990 cm^{-1}, CH_3 out-of-plane end asymmetric stretch at 3010 cm^{-1}, and unsaturated =CH stretch at 3028 cm^{-1}. The two dominant bands of the up-to-five Raman bands in the 2940–3030 cm^{-1} region have a consistent band spacing of 25 cm^{-1} in all four aerosols. Finally we discuss improvements to the PTRS that should provide a system which can trap a higher fraction of particle types and obtain Raman spectra over a larger range (e.g., 200–3600 cm^{-1}) than those achieved here.

Published by Elsevier Ltd.

1. Introduction

Biological particles (bioaerosols) in the atmosphere include primary biological aerosol particles (PBAP) such as bacteria, fungal spores, plant pollens, and small fragments of plants or fungi, and secondary bioaerosols such as those formed by ozone-initiated polymerization of terpenes. PBAP can transmit diseases of humans (e.g., inhalation anthrax) or plants (e.g., smuts, rusts); act as allergens (e.g., pollens, or dried proteins from cat saliva); affect climate by absorbing and/or emitting light; and change clouds and precipitation patterns by acting as condensation nuclei. There is a need for improved methods to rapidly characterize atmospheric bioaerosols.

* Corresponding author.
E-mail address: yongle.pan.civ@mail.mil (Y.-L. Pan).

http://dx.doi.org/10.1016/j.jqsrt.2014.11.004
0022-4073/Published by Elsevier Ltd.

Several optical techniques which require no reagents have been developed and used for bioaerosol detection, partial characterization, or in some cases identification, depending upon the type of bioaerosol, the technique or combination of techniques used. For air samples collected onto a surface these techniques include optical and electron microscopy [1]; fluorescence microscopy and spectroscopy; Raman spectroscopy; and combinations of Raman spectroscopy and imaging [2]. Optical and electron microscopy provide information on the size, shape, and surface structure of a particle. X-ray fluorescence, which is often available with electron microscopes, provides information on the atomic composition. The combination of Raman spectroscopy with optical imaging offers information on types of chemical bonds and types of chemicals and biochemical molecules in particles. Instruments have been developed for particles in air samples which pass through an instrument, where the particles are not collected but are carried through the instrument in flowing air. Some of these instruments measure single particle elastic scattering, and/or single particle fluorescence, and/or laser- or spark-induced breakdown spectroscopy (LIBS/SIBS) and some are commercially available [3]. Laser induced fluorescence (LIF), especially dual-wavelength UV-LIF has been demonstrated for near-real time detection and partial classification of bioaerosols particles [4–9]. The technique was shown to be capable of differentiating pollens from various plant species [9,10]. Fluorescence clustering analysis, especially when it is combined with the dual-wavelength UV-LIF, appears promising for rapid airborne bioaerosol characterization [11,12]. When excited at a visible wavelength, e.g., 488 nm, 515 nm, 633 nm, or 780 nm, most pollens and fungal spores have one or several fluorescence humps in a wide spectral range, e.g., 500–800 nm. These relatively structureless fluorescence spectra usually lack discriminating signatures for chemical characterization of bioaerosols. LIBS, which characterizes the elemental composition of a particle, has also been used to study a pollen particles one-at-a-time [13]. Bioaerosols tend to be highly complex, and their fluorescence, Raman, or breakdown spectra may depend upon how a sample is grown, washed, dried, stored, and/or processed in the atmosphere by sunlight, ozone, etc.

Here we are particularly interested in methods which can be used to measure samples one-at-a-time as particles flow in air or are stably trapped in air. Raman scattering can be far more informative than elastic scattering or fluorescence. Pollens are a special case where the elastic scattering used in optical microscopy can in many cases be used for identification. Raman spectroscopy is well suited for bioaerosol characterization and even possible identification in cases where the composition of all the relevant aerosol particles that could reach a sampler in some location is known. Raman spectra of many materials can be so sensitive to the chemical constituents (e.g., proteins, DNA, RNA, fatty acids, fats, cellulose, sporopollenin, chitin, lignin), and their molecular structures that in many cases these spectra can be used as “fingerprints” to identify chemical species and even biological species [14–16]. Also, how these Raman spectra change as bioaerosols or other particles are modified by their environment is also of interest. A pollen, plant or fungal spore typically contains many thousands of molecules and numerous chemical functional groups. Their Raman spectra exhibit Raman bands (structures or peaks) that are related to vibrational modes of individual chemical groups. For example, in low spectral resolution or not-well-resolved Raman spectra of pollens, Raman bands attributed to different vibrational modes of sporopollenin (a carotenoid-like aliphatic polymer) consisting of aromatic or conjugated side chains dominate the spectra [17–25]. They have peaks at $\sim$600 cm^{-1} from aromatic ring deformation [18]; $\sim$1000 cm^{-1} from breathing mode of the trigonal ring [18–19]; $\sim$1080 cm^{-1} from the C–C skeletal vibrations [18–19]; $\sim$1600 cm^{-1} from ring stretches of phenyl structures [17–18]; $\sim$1440 cm^{-1} from C–H_2 deformation [17–19]; and $\sim$2900 cm^{-1} from CH_2 and CH_3 stretches [18]. Exemplar protein bands are at $\sim$1650 cm^{-1} from C=O stretch of the amide I system [18–20]; $\sim$1520 cm^{-1} from N–H stretch of the amide II; $\sim$1300 cm^{-1} from N–H and C–H deformation of the amide III [18–20]. Phenylalanine may have Raman bands at $\sim$600, 1000, and 1600 cm^{-1} [22]. Tryptophan and tyrosine have a band at $\sim$1166 cm^{-1} [23]. Nucleic acids may also have Raman bands at $\sim$820 cm^{-1} from C–O–P–O–C in RNA backbone; $\sim$1166 cm^{-1} from guanine; $\sim$1360 cm^{-1} from adenine and guanine; $\sim$1565 cm^{-1} from adenine and guanine. Cytosine and uracil have weak vibrations at $\sim$790 cm^{-1} [18–20]. Therefore, Raman spectra can be used for characterization of chemical compositions in bioaerosols. On the other hand, some of Raman bands have similar Raman shifts, because common molecular groups are included in different pollens. And the same chemical species (functional group) may have a series of Raman bands in different locations, e.g., triolein and trilionlenin have Raman bands at 970, 1065, 1081, 1121, 1302, 1440, and 1656 cm^{-1}[22]; oleic acids have bands at 1036, 1302, and 1440 cm^{-1}; carotenoid have bands at 1522, 1189, 1156 cm^{-1} [25], etc. Therefore, compared with chemical characterization, it is more challenging to achieve pollen/spore identification using specific Raman bands. For some studies of Raman spectra of pollens and spores the particles are laid on a substrate and spectra are recorded using a Raman spectrometer (e.g., [25,26]). In those studies, a Raman excitation laser beam was scanned across each micro-size (15–60 μm) pollen particle with a spatial resolution of 1 μm. About 16 weak Raman bands were indentified for each of the 15 pollens in a Raman shift range of 400–1600 cm^{-1}. The results showed some promise for pollen classification, and some Raman bands have been identified as signatures of pollen components. Guedes et al. [27] measured Raman spectra of 34 different airborne pollens using a Raman spectrometer toward the ambitious goal of developing a “pollen Raman spectra database”. Each of the pollen spectra shows up to 20 Raman bands superposed on the top of a strong fluorescence background in the Raman shift range of 500–1800 cm^{-1}. Most bands are broad and very weak; only a few have a sharp peak. Similar spectral features (approximately the same number of Raman bands and the same fluorescence interference) in the spectral range of 500–1800 cm^{-1} were also reported in an earlier study of

single allergy-related pollen particles [28]. In that work reduction of fluorescence interference by using different excitation wavelengths (514 nm, 633 nm, and 780 nm) was also investigated.

A key problem with measuring Raman spectra from particles in air is that Raman scattering tends to be so weak that the required acquisition times are longer than the time it takes for a particle to move through a typical sample volume. Therefore, a method to hold the particles in air is needed. Electric forces generated using three electrodes to counteract gravity were first reported to hold particles stably in air 100 years ago [29]. Electrodynamic traps (also called electrodynamic balance devices (EDBs)) were developed in the 1950s [30]. EDBs have been used extensively for studies of particles trapped in air, including studies of changes in particle composition (e.g., [30,31]) and Raman spectra of bioaerosol particles trapped from the atmosphere [32].

Optical tweezers have been widely used for manipulation of micro- or nano-size particles for physical, chemical, and or biological characterization [33–35]. The optical-tweezers technique is often combined with another technique, e.g., Raman spectroscopy, to make optical tweezers-Raman spectroscopy, to further broaden its application in many research fields [36–43]. In optical tweezers-Raman spectroscopy, a micro-size species is trapped, typically in an aqueous solution but much less commonly in air, by photon radiation force (RF). The measured Raman spectra are related to the optical, physical, and chemical properties of the species, and even to the properties of its surrounding media, e.g., the solution. Optical tweezers-Raman spectroscopy has been used for spectroscopic studies of a wide variety of species. A limitation of the technique as commonly employed (e.g., in a liquid) is that a particle is trapped in a liquid. Another limitation for RF trapping (either liquid or gas) is that the material of the particle must be optically transparent (non-absorbing) [37–43]. This limitation leaves the light-absorbing species, e.g., pollens, spores, and/or chemically soluble species, barely explored with the optical tweezers-Raman spectroscopy technique.

Photophoretic trapping-Raman spectroscopy (PTRS) is being developed for studying strongly-absorbing, absorbing or weakly-absorbing species in air [44]. In PTRS, a light-absorbing particle is trapped in air mainly by photophoretic forces that can be up to 10^5 times stronger than RF [45–47]. While the RF force results from the direct transfer of momentum from scattered or absorbed photons, the photophoretic force results indirectly from a particle absorbing photons in a spatially non-uniform manner leading to a non-uniform temperature at the particle surface. Gas molecules on the higher temperature side of the particle tend to collide with the particle at higher velocity, imparting a net force pushing the particle in the direction of its colder side. In addition to the RF and photophoretic force, absorbing particles can also experience a convective force, even with no externally applied airflow, in which a particle can heat the surrounding gas, causing the gas molecules to rise, thereby imparting a drag force on the particle in the vertical direction (i.e. against gravity). The relative strength of these forces depends on the absorptivity of the particle, the thermal conductivity of the particle, and the particle morphology, on the pressure and thermal conductivity of the surrounding gas, and on the strength and geometry of the optical field. Previous studies found that for strongly absorbing particles such as carbon nanofoam, the photophoretic force can be orders of magnitude stronger than the radiative force [48]. We performed an initial estimation assuming homogenous spherical particles illuminated by a plane wave using the approximations and derivations in Ref. [45–52]. We used Eq. (1) from Ref. [51] for the photophoretic force and Eq. (28) from Ref. [49] for the free convective force. This expression for the free convective force is a curve fit based on particles in the 65–150 μm diameter range and which we use to extrapolate to smaller particles. We calculated forces for particles with a thermal conductivity of 0.159 W/m/K and an absorption length of 2 μm. Using these expressions and particle compositions we found that the photophoretic force was ~2 orders of magnitude stronger than either the radiative force or the convective force for the range of particle sizes (5–40 μm diameter) observed in this work. A detailed calculation of the relative strength of these forces in the bi-directional trapping geometry used in this work will be reported in a future study. Nonetheless, based on this estimation of forces, and on observations of ourselves and of others (e.g., Arnold et al., and Shvedov et al.), we think that the photophoretic force is the dominant force in the particle trapping approach investigated in this work.

In this PTRS technique, the Raman signal is collected with a high N.A. microscope-objective lens and then dispersed by a spectrograph. The PTRS technique was first demonstrated in 2012 by recording Raman spectra of strongly-absorbing carbon nanoparticles trapped in air [44]. In this work, we extend the PTRS technique to study absorbing and weakly-absorbing bioaerosols (pollens and fungal spores) photophoretically trapped in air, and show PTRS spectra of pollens and spores in the Raman shift region of 1600–3400 cm^{-1}.

Characterization of an individual pollen particle suspended in air may provide more insight into a particle' chemical and biological composition than many other techniques. This is because: (1) The compositions of pollens, spores and other bioparticles in the atmosphere can be highly complex with diverse physical properties. (2) A study of a single pollen particle in air has no potential interference from other airborne particles and no optical interference from its support media (e.g., a sample substrate). (3) A pollen particle in air is free from chemical interactions (dissolving in it or changing in shape in response to its properties) with the liquid it is suspended in. (4) A study of single pollen particle yields *the particle* information, instead of particle-averaged information and so allows the determination of minority species within a group of otherwise very similar appearing particles. (5) A dry particle may grow in size as it takes up water as the humidity increases and/or the temperature decreases, and particles may lose mass, e.g., by evaporation of volatile organic compounds. (6) A particle may change its surface structure, react with gases (e.g., ozone or oxides of nitrogen) introduced into the chamber to investigate

processes that might occur in the atmosphere, etc. A complete time-evolution profile can be investigated by observing the same single particle over the entire period of study. This type of single particle study requires very demanding capabilities of a technique, as demonstrated in this work.

In this paper, we describe a PTRS system (Section 2) that is employed to study Raman spectra of single pollen/spore particles trapped in air. Raman spectra of pollens from three plant species and one species of fungal spore are presented in Section 3. A brief discussion of real-time bioaerosol particle characterization using the PTRS technique combined with an innovative sampling-trapping-releasing device is given in the concluding remarks (Section 4).

2. Experimental arrangements

2.1. Optical configuration for photophoretic trapping

Fig. 1(a) illustrates the key optical configurations of the photophoretic trapping-Raman spectroscopy system, which is similar to the experimental setup described in Ref. [44], except that a particle here is trapped in a closed quartz cell. A linearly polarized Gaussian beam at 488 nm from a continuous-wave argon ion laser (Coherent Inc., Innova 300C) was used. After reforming and expanding the laser beam using a telescope consisting of a pair of lenses (f=25 mm and 180 mm) and a pinhole (D=500 μm), the collimated and visually uniform circular beam with a diameter of 15 mm passed through a pair of identical axicons separated by 500 mm (Del Mar Photonics, cone angle=175°) and a circular hollow beam of 20 mm in diameter was formed. The hollow beam was split into two beams with horizontal and vertical polarizations respectively using a polarization beam splitter cube. The two counter-propagating beams were focused by two identical micro objective lenses (MO1 and MO2, Nikon, ELWD 20×, N.A.=0.4), as illustrated in Fig. 1(b), to form two optical cones inside the quartz cell and form, in the region between the two vertexes, a low-light intensity volume enclosed by a high intensity surface, e.g., the overlapped region at the cone vertex [44,53]. Although the nearly identical laser power in each of the two beams was known, the exact power applied to the trapping or to the Raman excitation was unknown, as the laser beams did not directly shine on the trapped particle in the closed trapping region. As shown in Fig. 1(b), a single weakly-absorbing English oak pollen (30.0–34.0 μm) particle was trapped in the overlapped region stably. Particle shape, position, or motion was continuously monitored using a CCD camera (Pulnix TM-9701) during an entire trapping period. Fig. 1(c) presents some images of the trapped particles; they are single wall carbon nanotubes (SWCNT), English oak, ragweed, ryegrass, and Bermuda grass smut spores from the left to the right in order. The size of each image was not scaled to the size of each particle. Rather, the images show some differences in shape and light scattering effect among the particles. For instance, the shape of the trapped SWCNT appears to be spherical while the particle ensemble of Bermuda grass smut spores has an irregular shape.

2.2. Setup of the Raman spectral system

Raman signal along with the elastic scattering from the trapped particle was collected through a micro-objective lens (MO3, Creative Device, f=20 mm, 50×, N.A.=0.42). The elastic scattering light at 488 nm was filtered out by a dichroic mirror and further eliminated by a long-pass filter (Semrock LP02-488RE-25). The Raman signal was dispersed by a spectrograph (Acton, SP2300, grating 1200/mm, blaze 500 nm), and recorded by an electron multiplying charge coupled device (EMCCD, Princeton, ProEM 1600×200). The entrance slit width was set at 50–400 μm. The gain of the EMCCD was adjustable in the range of 1–100. The highest gain used in the experiments was 50. The spectral integration time was chosen between 10 s and up to 10 min, depending on Raman signal intensity and different sample species. Wavenumber readings in the spectrograph were calibrated by using Raman shifts of atmospheric nitrogen and oxygen.

2.3. Bioaerosol species and single wall carbon nanotubes (SWCNT)

Three different pollens and one species of fungal spores were studied. Their single particle sizes are 30.0–34.0 μm (English oak pollen, *Quercus robar*, purchased from Greer Labs); 18.7–23.8 μm (ragweed pollen, *Ambrosia* sp., purchased from Duke Scientific); 32.2–41.8 μm (ryegrass pollen, *Lolium perenne*, collected in Southern California, USA [10]); 5.6–8.2 μm (Bermuda grass smut spores, *Ustilago cynodontis*, purchased from Duke Scientific). Graphitized single wall carbon nanotubes (SWCNT) were purchased from Thermal Scientific Inc.

3. Results and discussion

3.1. Wavenumber calibration of the experimental system using Raman spectra of atmospheric O_2 and N_2

Fig. 2 shows Raman spectra of atmospheric air taken with the trapping cell empty. The oxygen and nitrogen bands in the spectra were used for wavenumber calibration of the experimental system. The entrance slit of the spectrograph was set at 50 μm in order to obtain a narrow band for a better accuracy of wavenumber. The EMCCD gain was set at 1 (the minimal level) and the integration time was 2 min. The full widths at half maximum (FWHM) for the O_2 band at 1558 cm^{-1} was 8 cm^{-1} and for N_2 at 2331 cm^{-1} was 5 cm^{-1} [14]. Therefore Raman shifts of the spectra below calibrated using these oxygen and nitrogen bands will have a wavenumber accuracy of ± 4 cm^{-1} (the half of the FWHM of the O_2 band).

3.2. PTRS spectra of SWCNT particles trapped in air

Fig. 3 shows a typical Raman spectrum of SWCNT particles trapped in air. The spectrum shows three Raman bands at 1367, 1585, and 2714 cm^{-1} that are attributed to carbon. The peak at 1585 cm^{-1} belongs to the G-band of SWCNT, which typically has two main components at 1570 cm^{-1} and 1590 cm^{-1} associated with vibrations of

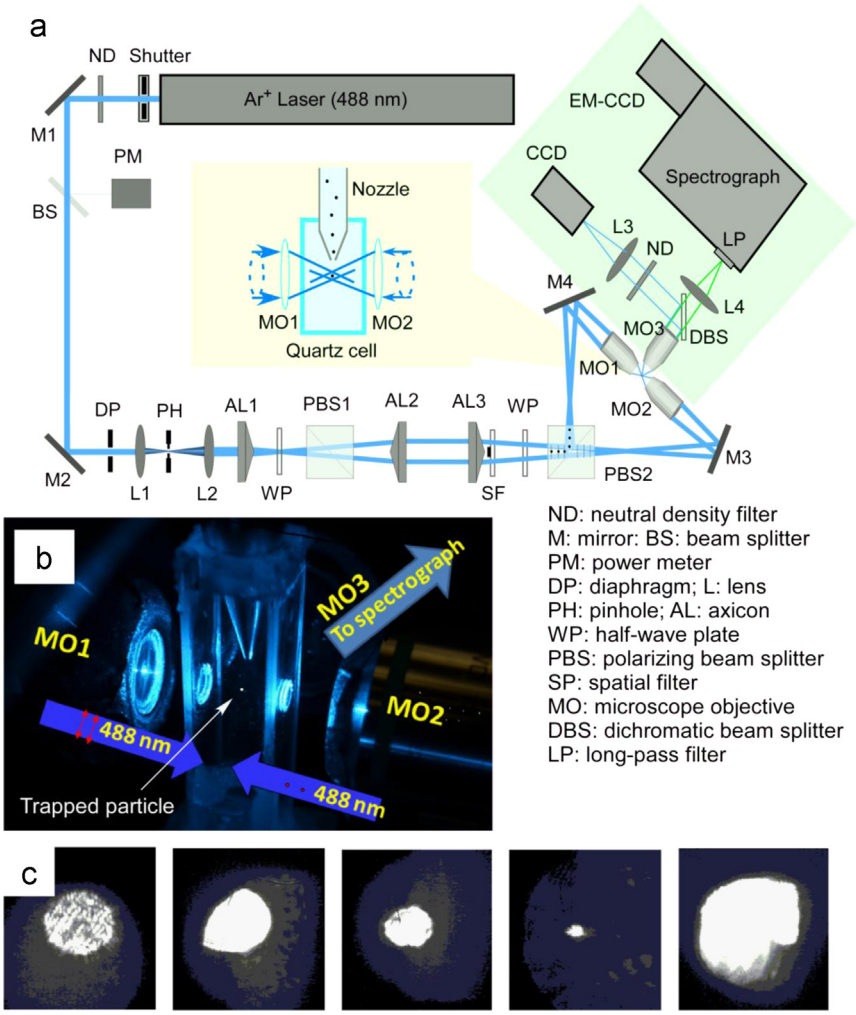

Fig. 1. Schematic of the photophoretic trapping-Raman spectroscopy (PTRS) system: (a) optical arrangements; (b) an image of the key trapping components and the location of the trapped particle; and (c) images of trapped particles, from the left to the right: single wall carbon nanotubes (SWCNT), English oak, ragweed, ryegrass, and Bermuda grass smut spores.

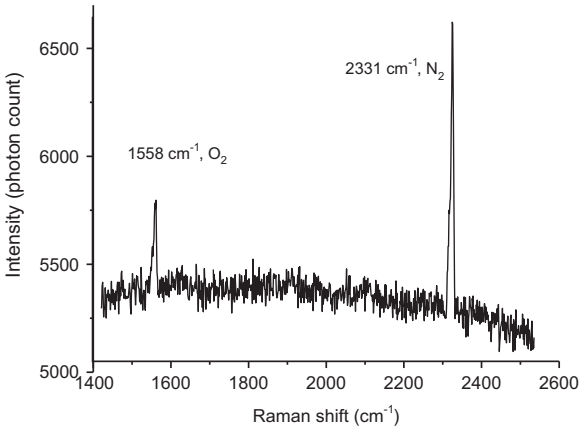

Fig. 2. Raman spectra of ambient O_2 and N_2 recorded for wavenumber calibration of the photophoretic trapping Raman spectroscopy system. The excitation wavelength was 488 nm. The entrance slit width of the spectrograph was 50 μm.

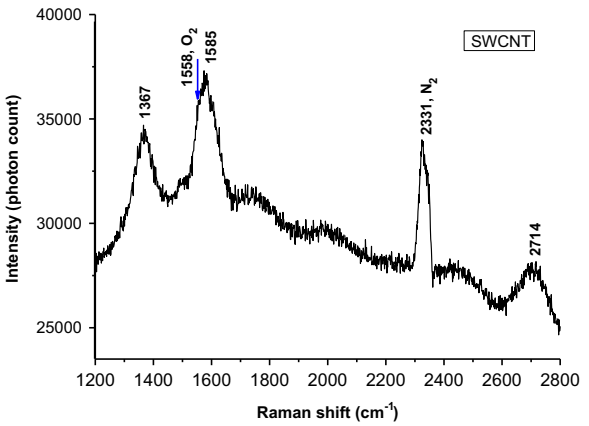

Fig. 3. Photophoretic trapping Raman spectra of a single particle ensemble of graphitized single wall carbon nanotubes (SWCNT) trapped in air in the closed quartz cell.

carbon atoms along the circumferential direction and the nanotubes axis direction, respectively. These two components are not shown in the peak at 1585 cm^{-1} in Fig. 3. The small shoulder on the left side of the peak is the contribution from the O_2 band. The peaks at 1367 and 2714 cm^{-1} are the D-band and G′-band, respectively, of graphite-like materials through a double resonance process [54]. The first two Raman bands at 1367 and 1585 cm^{-1} were also reported in our previous study that demonstrated the PTRS technique for trapped carbon nanotubes [44]. All of the three carbon Raman bands were also reported in a similar study of trapped carbon particles using a single laser beam trapping scheme [55]. The identifications and assignments of the three carbon Raman bands as well as the oxygen and nitrogen bands shown in Fig. 3 indicate that the PTRS system was functional and ready to be used for exploration of PTRS spectra of absorbing and weakly-absorbing bioaerosol particles trapped in air.

3.3. PTRS spectra of a single particle ensemble of Bermuda grass smut spores

Bermuda grass smut spores are black and can be readily trapped in air by photophoretic forces. Fig. 4 shows PTRS spectra of two individually trapped particles. Overall the spectra are quite reproducible: the background Raman band of N_2, a spectral peak near 2949 cm^{-1}, and the hump-like fluorescence in the spectral shift range of 1550–3450 cm^{-1}. In a previous study of single particle Raman of pollens and fungal spores [31], in that case excited at 514 nm, the spectra have five broad Raman peaks in the spectral range of 800–1600 cm^{-1}, in addition to the peak around 2949 cm^{-1} that is attributed to the C—H stretch (more details in Section 3.4). In Fig. 4, except for the N_2 band, there is no Raman band in the spectral shift region from 1600 to 2850 cm^{-1}; this is the same feature as reported in the literature [28,31]. No obvious effect on the fluorescence reduction was observed after more than two hours continuous light illumination on the trapped particle.

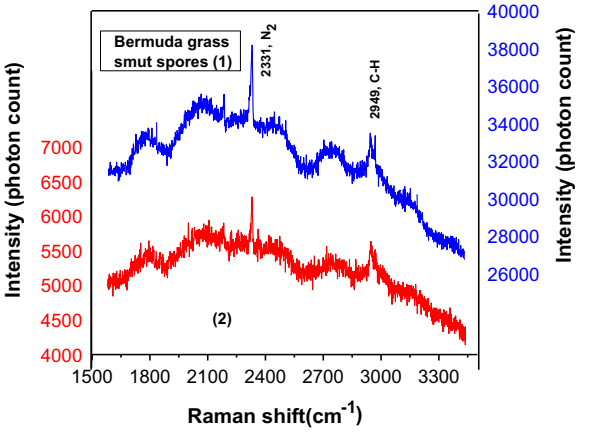

Fig. 4. Demonstration of PTRS spectra for single Bermuda grass smut spores (6.2–8.9 μm) trapped in air. (1) and (2) denote the spectra from two individual traps.

3.4. Comparison of PTRS spectra of three pollens and one type of fungal spore trapped in air

The pollens we examined, which are light yellow and brown, appear to absorb much less light than do the carbon nanotubes or Bermuda grass smut spores, which are dark black. Using the photophoretic trapping scheme (Fig. 1) it is more difficult to trap a pollen particle than to trap the strongly-absorbing (e.g., SWCNT) and absorbing particles (e.g., Bermuda grass smut spores). When trapping weakly-absorbing pollen particles, we expect that the dominant trapping force is still the thermal-based photophoretic force, but the radiation pressure force is relatively more significant. In the experiments, we tried more than 10 different pollens that were in a size range of 10–47 μm and only some of them were successfully trapped under the same experimental conditions (the same alignments, laser power, laser wavelength, and the method of particle introduction into the trapping cell). In particular, English oak (*Q. robur*), black oak (*Quercus velutina*), black walnut (*Juglans nigra*), pecan (*Carya illinoensis*), ragweed (*Ambrosia*), ryegrass (*L. perenne*), and paper mulberry (*Broussonetia papyrifera*) pollens were successfully trapped using the trapping scheme in Fig. 1. A pollen particle, once it was trapped, could typically be held stably for as long as desired, e.g., up to eight hours in this work.

Fig. 5 shows Raman spectra of trapped individual bioaerosol particles: (A) English oak pollen, (B) ragweed pollen, (C) ryegrass pollen, and (D) Bermuda grass smut spores. Overall the spectra have similar profiles with a strong peak at approximately 2949 cm^{-1} and nitrogen band at 2331 cm^{-1}. The emission between 1600 and 2700 cm^{-1} is remarkably high compared with most spectra of biological cells, proteins, nucleic acids, lipids, etc., when they are excited at wavelengths that generate less fluorescence. Light at 488 nm is known to excite relatively strong fluorescence in bacteria and tree leaves [8]. Sporopollenin in pollens and fungal spores is reported to fluoresce in the 400–650 nm range with high fluorescence intensity when excited at 300–550 nm [56,57]. Flavins are likely to be a main contributor to the fluorescence in the 500–580 nm range in bacteria, but probably contribute a much smaller fraction of the fluorescence in this range in pollens and fungal spores because they have many other fluorescent molecules [56,57].

In comparing the spectra of the different species it is important to note that the fungal spore signal relative to the air-nitrogen peak is approximately 10 times smaller than it is for any of the pollens. The main cause of this difference is probably that the fungal spores are so much smaller than the pollens. Depending upon the species, one to five Raman peaks can be seen. Up to five bands are identified in the three pollens and only two bands appear in the fungal spores. Because the Raman signal relative to the fluorescence background and noise is smaller for the fungal spore, it is difficult to assign this difference to the diversity in species.

The four spectra in Fig. 5 can be classified into two groups, e.g., spectra of pollen and spectra of spores, based on the spectral differences and similarities. First, the

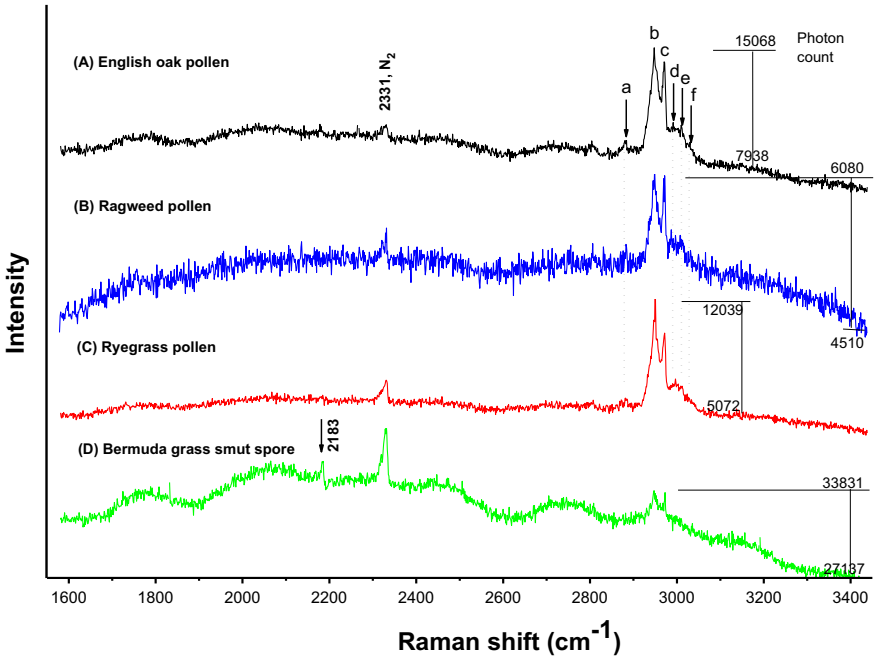

Fig. 5. Demonstration of PTRS spectra of single pollens and comparison of Raman spectra of the pollens and the fungal spores trapped in air. The spectrum in (A), (B), (C) or (D) is from one particle trapped. The numbers shown on the right side of each spectrum denotes actual photon counts. The CCD integration times used in for the spectra in (A), (B), (C), and (D) were 60 s, 30 s, 60 s, and 30 s respectively. The gain of the CCD was set 2.

particle's Raman signal relative to the background noise and fluorescence is roughly 10 times smaller for the fungal spores than that for the pollens under the conditions used to obtain the spectra in Fig. 5. Because of this, some of the other classification features may be less a function of the intrinsic Raman spectra or biochemical features of the particles, but be more a function of signal to background in this system. Second, all the pollen spectra have a Raman band at 2878 cm^{-1}, as marked by 'a' in the spectrum (Fig. 5(A)). Third, five recognizable bands: b, c, d, e, and f with Raman shifts of 2948, 2970, 2990, 3010, and 3028 cm^{-1} respectively can be noticed in the pollen spectra in Fig. 5. The primary bands marked as b and c have a consistent separation of 25 ± 1 cm^{-1} in all three pollens. Fourth, unlike the spectra of pollens, the Raman spectrum of Bermuda grass smut spores has an additional peak at 2183 cm^{-1} that remains unassigned in this work. Furthermore, the big peak in the spectrum (Fig. 5(D)) appears to have two main components only.

The Raman scattering near the peak in Fig. 5 is probably primarily attributable to sporopollenin and lipids that are common in pollens and fungal spores. Both Refs. [28,31] reported a similar Raman peak near 2949 cm^{-1}. The peak profiles shown in those two studies are similar, with a smooth and sharp edge in the longer wavenumber side and a small shoulder on the shorter wavenumber side. No fine peak structures were resolved. However, the peak profile observed in the present work is inverted from that of those earlier reports. The profiles in Fig. 5 have a sharp rising edge on the shorter wavenumber side, and resolved peak structures on the longer wavenumber side. The peak profile observed here is similar to the profiles (with shoulder structures on the longer wavenumber side) of the Raman spectra of *Bacillus anthracis* (*Ba*), *B.cereus* (*Bc*), *B. globigii* (*Bg*), and *B. thuringiensis* (*Bt*) measured using Raman chemical imaging microscopy [58]. Similarly, Raman spectra of waterborne pathogens also have this shoulder on the longer wavenumber side [59]. In a recent study, Raman spectroscopy was used to detect anthrax endospores in powder samples [60], the Raman spectra of particles of powdered milk (fat and starch) and 3-hydroxybutyrate (poly) also have the shoulder structures on the longer wavenumber side (inverted from the peak structure reported in Refs. [28,31]). Comparison of the peak structures shown in Fig. 5 with the structures of Raman spectra of hydrocarbons from a Bunsen burner [61] supports the idea that the peak structures shown in Fig. 5 are different from those reported in the Raman spectra of pollen/spores [28,31]. One common feature of the Raman spectra of photophoretically trapped pollens/spores and the Raman spectra of hydrocarbons from a Bunsen burner is the elevated temperatures of the molecules of interest. Molecules in the photophoretically trapped particles have elevated temperature due to absorption of the light. In a Raman study of human brain lipids, Krafft et al. [62] reported seven Raman bands in the wavenumber region of 2700–3500 cm^{-1}. They characterized the peak near 2949 cm^{-1} into 12 difference peak structures (cases). Of the 12 different cases, seven have the five-band structures with two dominant bands and three minor bands on the longer wavenumber side, similar to the ones shown in A–C in Fig. 5. One of the 12 cases has the two-band structures that are the same as in the spectrum D of Fig. 5. One major difference between the spectra shown in Fig. 5 and the Raman spectra of human lipids reported in Ref. [59] is that the positions of the five Raman bands in Fig. 5 shifted to

the longer wavenumber side by ~20–100 cm^{-1}. This wavenumber difference is not due to uncertainty in the wavenumber readings, but is due to different chemical compositions and experimental conditions. Here the five bands (b, c, d, e, and f) shown in Fig. 5 are tentatively assigned to the CH_2 symmetric stretch at 2948 cm^{-1}, the CH_2 Fermi resonance stretch at 2970 cm^{-1}, the CH_3 symmetric stretch at 2990 cm^{-1}, the CH_3 out-of-plane end asymmetric stretch at 3010 cm^{-1}, and the unsaturated =CH stretch at 3028 cm^{-1}. It is not clear why the peak in the Raman spectrum of the Bermuda grass smut spores has only two main components, or why the Raman spectrum of these spores lacks the peak marked at position a. Is it simply because other three bands and the peak marked at 'a' are considerably weaker and so do not appear against the high fluorescence background in this spectrum? The spectra shown here are the first Raman spectra of pollens and fungal spores obtained using PTRS. Their spectral range is small enough that they are not very convincing as to the use of Raman spectral features for discriminating among pollens and spores. However, these PTRS spectra have different spectral features, and they suggest the potential usefulness of improving the PTRS technique to obtain spectra with larger spectral ranges and less fluorescence.

4. Concluding remarks

A method of rapid and accurate characterization and identification of biological aerosol particles in air is highly desired. Raman spectroscopy combined with rapid methods for trapping particles [63] is one of the promising techniques to explore. In this work, we have combined photophoretic [44,48,51,52,63] trapping and Raman spectroscopy to characterize single bioaerosol particles in air. In particular, a single light absorbing pollen or fungal spore is trapped in air by photophoretic forces, and Raman spectroscopy is used as an interrogator, to form photophoretic trapping Raman spectroscopy (PTRS). Here, PTRS is used to characterize three pollens (English oak, ragweed, and ryegrass) and one fungal spore (Bermuda grass smut spores). The PTRS spectra of the four species recorded in the spectral shift range of 1600–3400 cm^{-1} show one large spectral peak that contains five Raman bands for the three pollens and two bands for Bermuda grass smut spores. In this spectral region, Raman spectra of the three pollens are similar, but they are different from the Raman spectrum of the spores, probably in part because the spores are much smaller than the pollens, and their Raman signal relative to background is smaller. The five Raman bands in the peak region are tentatively assigned to the CH_2 symmetric stretch at 2948 cm^{-1}, the CH_2 Fermi resonance stretch at 2970 cm^{-1}, the CH_3 symmetric stretch at 2990 cm^{-1}, the CH_3 out-of-plane end asymmetric stretch at 3010 cm^{-1}, and the unsaturated =CH stretch at 3028 cm^{-1}.

This work demonstrates the first application of the PTRS technique to the study of absorbing and weakly-absorbing single bioaerosol particles trapped in air. The structured Raman spectra of the trapped pollens and spores suggest that the PTRS technique can be applied to characterization of single pollen and fungal particles in air. Future work is needed to improve the optical system to obtain Raman spectra in the low-wavenumber region, e.g., 400–1600 cm^{-1} where bioaersols have more characteristic Raman bands [28]. The spectral integration times used in this work are relatively long (40 s to a few min). An additional excitation laser beam at a wavelength different from the trapping beam may be used to directly illuminate the trapped particle to increase the Raman scattering signal intensity, and, in the case of a different excitation wavelength, to reduce the fluorescence. Given the significant stride that has been made in technology for continuously sampling-trapping-and-releasing of successively arriving particles in air [63], it is conceivable that it will be possible to develop a near-real time airborne bioaerosol particle characterization instrument using the PTRS technique combined with the novel trapping technique.

Acknowledgments

This research was supported by the Defense Threat Reduction Agency (DTRA) under Contract number HDTRA136477 and HDTRA1310184, US Army Research Laboratory mission funds, and US Army Research Office Grants W911NF-13-1-0429 and W911NF-13-1-0297.

References

[1] Weber RW. Ann Allergy 1998;80:141–5.
[2] Tripathi A, Jabbour RE. Bioaerosol analysis with Raman chemical imaging microspectroscopy. Anal Chem 2009;81:6981–90.
[3] Cross ES, Onasch TB, Canagaratna M, Jayne JT, Kimmel J, Yu X-Y, et al. Single particle characterization using a light scattering module coupled to a time-of-flight aerosol mass spectrometer. Atmos Chem Phys 2009;9:7769–93.
[4] Pinnick RG, Hill SC, Nachman P, Videen G, Chen G, Chang RK. Aerosol fluorescence spectrum analyzer for rapid measurement of single micrometer-sized airborne biological particles. Aerosol Sci Technol 1998;28:95–104.
[5] Pan YL, Hartings J, Pinnick RG, Hill SC, Halverson J. Single-particle fluorescence spectrometer for ambient aerosols. Aerosol Sci Technol 2003;37:628–39.
[6] Pan YL, Pinnick RG, Hill SC, Rosen JM, Chang RK. Single-particle laser induced-fluorescence spectra of biological and other organic-carbon aerosols in the atmosphere: measurements at New Haven, CT and Las Cruces, NM, USA. J Geophys Res 2007;112:D24S19.
[7] Pan YL, Hill SC, Pinnick RG, Huang H, Bottiger JR, Chang RK. Fluorescence spectra of atmospheric aerosol particles measured using one or two excitation wavelengths: comparison of classification schemes employing different emission and scattering results. Opt Express 2010;18:12436–57.
[8] Hill SC, Pinnick RG, Nachman P, Chen G, Chang RK, Mayo MW, et al. Aerosol-fluorescence spectrum analyzer: real-time measurement of emission spectra of airborne biological particles. Appl Opt 1995;34:7149–55.
[9] Mitsumoto K, Yabusaki K, Kobayashi K, Aoyagi H. Development of a novel real-time pollen-sorting counter using species-specific pollen autofluorescence. Aerobiologia 2010;26:99 (-11).
[10] Pan YL, Hill SC, Pinnick RG, House JM, Flagan RC, Chang RK. Dual-excitation-wavelength fluorescence spectra and elastic scattering for differentiation of single airborne pollen and fungal particles. Atmos Environ 2011;45:1555–63.
[11] Pinnick RG, Fernandez E, Rosen JM, Hill SC, Wang Y, Pan YL. Fluorescence spectra and elastic scattering characteristics of atmospheric aerosol in Las Cruces, New Mexico, USA: variability of concentrations and possible constituents and sources of particles in various spectral clusters. Atmos Environ 2013;65:195–204.

[12] Robinson NH, Allan JD, Huffman JA, Kaye PH, Foot VE, Gallagher M. Cluster analysis of WIBS single-particle bioaerosol data. Atmos Meas Tech 2013;6:337–47.
[13] Boyain-Goitia AR, Beddows DCS, Griffiths BC, Telle HH. Single-pollen analysis by laser-induced breakdown spectroscopy and Raman microscope. Appl Opt 2003;42:6119–32.
[14] Herzberg G. Molecular spectra and molecular structure: infrared and Raman spectra of polyatomic molecules, vol. II. Prentice-Hall; 1945.
[15] Rodgers KR, Spiro TG. Nanosecond dynamics of the R–T transition in hemoglobin: ultraviolet Raman studies. Science 1994;265:1697–9.
[16] Xie C, Mace J, Dinno MA, Li YQ, Tang W, Newton RJ, et al. Identification of single bacterial cells in aqueous solution using confocal laser tweezers Raman spectroscopy. Anal Chem 2005;77:4390–7.
[17] Manoharan R, Ghiamati E, Britton KA, Nelson WH, Sperry JF. Resonance Raman spectra of aqueous pollen suspensions with 222.5–242.4-nm pulsed laser excitation. Appl Spectrosc 1991;45:307–11.
[18] Maquelin K, Kirschner C, Choo-Smith LP, van den Braak N, Endtz HP, Naumann D, et al. Identification of medically relevant microorganisms by vibrational spectroscopy. J Microbiol Method 2002;51:255–71.
[19] Schuster KC, Reese I, Urlaub E, Gapes JR, Lendl B. Multidimensional information on the chemical composition of single bacterial cells by confocal Raman microspectroscopy. Anal Chem 2000;72:5529–34.
[20] Maquelin K, Choo-Smith L-P, van Vreeswijk T, Endtz HP, Smith B, Bennett R, et al. Raman spectroscopic method for identification of clinically relevant microorganisms growing on solid culture medium. Anal Chem 2000;72:12–9.
[21] Manoharan R, Ghiamati E, Chadha S, Nelson WH, Sperry JF. Effect of cultural conditions on deep UV resonance Raman spectra of bacteria. Appl Spectrosc 1993;47:2145–50.
[22] De Gelder J, De Gussem K, Vandenabeele P, Moens L. Reference database of Raman spectra of biological molecules. J Raman Spectrosc 2007;38:1133–47.
[23] Pummer BG, Bauer H, Bernardi J, Chazallon B, Facq S, Lendl B, et al. Chemistry and morphology of dried-up pollen suspension residues. J Raman Spectrosc 2013;44:1654–8.
[24] Sengupta A, Brar N, Davis EJ. Bioaerosol detection and characterization by surface-enhanced Raman spectroscopy. J Colloid Interface Sci 2007;309:36–43.
[25] Schulte F, Lingott J, Panne U, Kneipp J. Chemical characterization and classification of pollen. Anal Chem 2008;80:9551–6.
[26] Schulte F, Jens M, Lothar WK, Panne U, Kneipp J. Characterization of pollen carotenoids with in situ and high-performance thin-layer chromatography supported resonant Raman spectroscopy. Anal Chem 2009;81:8426–33.
[27] Guedes A, Ribeiro H, Fernández-González M, Aira MJ, Abreu I. Cyanex based uranyl sensitive polymeric membrane electrodes. Talanta 2014;19:473–8.
[28] Ivleva NP, Niessner R, Panne U. Characterization and discrimination of pollen by Raman microscopy. Anal Bioanal Chem 2005;381:261–7.
[29] Arnold S. Spectroscopy of single levitated micron particles. In: Barber PW, Chang RK, editors. Optical Effects Associated with Small Particles. Singapore: World Scientific Publishing; 1988. p. 65–137.
[30] Wuerker RF, Shelton H, Langmuir RV. Electrodynamic containment of charged particles. J Appl Phys 1959;30:342–9.
[31] Laucks ML, Roll G, Schwei G, Davis EJ. Physical and chemical (Raman) characterization of bioaerosols—pollen. J Aerosol Sci 2000;31:307–19.
[32] Lee AKY, Chan CK. Single particle Raman spectroscopy for investigating atmospheric heterogeneous reactions of organic aerosols. Atmos Environ 2007;41:4611–21.
[33] Ashkin A. Acceleration and trapping of particles by radiation pressure. Phys Rev Lett 1970;24:156–9.
[34] Ashkin A. Applications of laser radiation pressure. Science 1980;210:1081–8.
[35] Ashkin A, Dziedzic JM, Bjorkholm JE, Chu S. Observation of a single-beam gradient force optical trap for dielectric particles. Opt Lett 1986;11:288–90.
[36] Tong L, Ramser K, Käll M. Optical tweezers for Raman spectroscopy. In: Kumar Challa SSR, editor. Raman spectroscopy for nanomaterials characterization. Heidelberg, Dordrecht, London, New York: Springer; 2012 ([Chapter 18]).
[37] Urlaub E, Lankers M, Hartmann I, Popp J, Trunk M, Kiefer W. Raman investigation of styrene polymerization in single optically trapped emulsion particles. Chem Phys Lett 1994;231:511–4.
[38] Ajito K, Torimitsu K. Near-infrared Raman spectroscopy of single particles. Trac-Trends Anal Chem 2001;20:255–62.
[39] Xie C, Dinno MA, Li Y. Near-infrared Raman spectroscopy of single optically trapped biological cells. Opt Lett 2002;27:249–51.
[40] Ajito K, Torimitsu K,K. Laser trapping and Raman spectroscopy of single cellular organelles in the nanometer range. Lab Chip 2002;2:11–4.
[41] Reid JP. Particle levitation and laboratory scattering. J Quant Spectrosc Radiat Transfer 2009;110:1293–306.
[42] Cherney DP, Harris JM. Confocal Raman microscopy of optical-trapped particles in liquids.Annual review of analytical chemistry, vol. 3. Palo Alto: Annual Reviews; 277–97.
[43] Chan JW, Esposito AP, Talley CE, Hollars CW, Lane SM, Huser T. Reagentless identification of single bacterial spores in aqueous solution by confocal laser tweezers Raman spectroscopy. Anal Chem 2004;76:599–603.
[44] Pan YL, Hill SC, Coleman M. Photophoretic trapping of absorbing particles in air and measurement of their single-particle Raman spectra. Opt Express 2012;20:5325–34.
[45] Rosen MH, Orr C. The photophoretic force. J Colloid Sci 1964;19:50–60.
[46] Arnold S, Lewittes M. Size dependence of the photophoretic force. J Appl Phys 1982;53:5314–9.
[47] Shvedov VG, Desyatnikov AS, Rode AV, Krolikowski W, Kivshar YS. Giant optical manipulation. Phys Rev Lett 2010;105:118103-1–4.
[48] Shvedov VG, Desyatnikov AS, Rode AV, Krolikowski W, Kivshar YS. Optical guiding of absorbing nanoclusters in air. Opt Express 2009;17:5743–57.
[49] Zhao B, Katoshevski D, Bar-Ziv E. Temperature determination of single micrometre-sized particles from forced/free convection and photophoresis. Meas Sci Tech 1999;10:1222–32.
[50] Horvath H. Photophoresis—a forgotten force? KONA Power Part J 2014;31:181–99.
[51] Desyatnikov AS, Shvedov VG, Rode AV, Krolikowski W, Kivshar YS. Photophoretic manipulation of absorbing aerosol particles with vortex beams: theory versus experiment. Opt Express 2009;17:8201–11.
[52] Shvedov VG, Hnatovsky C, Rode AV, Krolikowski W. Robust trapping and manipulation of airborne particles with a bottle beam. Opt Express 2011;19:17350–6.
[53] Wang C, Pan YL, Coleman M. Experimental observation of particle cones formed by optical trapping. Opt Lett 2014;39:2767–70.
[54] Dresselhausa MS, Dresselhausb G, Saitoc R, Joriod A. Raman spectroscopy of carbon nanotubes. Phys Rep 2005;409:47–99.
[55] Ling L, Li YQ. Measurement of Raman spectra of single airborne absorbing particles trapped by a single laser beam. Opt Lett 2013;38:416–8.
[56] Pöhlker C, Huffman JA, Pöschl U. Autofluorescence of atmospheric bioaerosols – fluorescent biomolecules and potential interferences. Atmos Meas Tech 2012;5:37–71.
[57] Pöhlker C, Huffman JA, Förster J-D, Pöschl U. Autofluorescence of atmospheric bioaerosols: spectral fingerprints and taxonomic trends of pollen. Atmos Meas Tech 2013;6:3369–92.
[58] Kalasinsky KS, Hadfield T, Shea AA, Kalasinsky VF, Nelson MP, Neiss J, et al. Raman chemical imaging spectroscopy reagentless detection and identification of pathogens: signature development and evaluation. Anal Chem 2007;79:2658–73.
[59] Tripathi A, Jabbour RE, Treado PJ, Neiss JH, Nelson MP, Jensen JL, et al. Waterborne pathogen detection using Raman spectroscopy. Appl Spectrosc 2008;62:1–9.
[60] Stçckel S, Meisel S, Elschner M, Rçsch P, Popp J. Raman spectroscopic detection of anthrax endospores in powder samples. Angew Chem Int Ed 2012;51:5339–42.
[61] Svanberg S. Atomic and molecular spectroscopy: basic aspects and practical applications. 4th ed.Springer; 4 December 2003.
[62] Krafft C, Neudert L, Simat T, Salzer R. Near infrared Raman spectra of human brain lipids. Spectrochim Acta Part A 2005;61:1529–35.
[63] Pan YL, Wang C, Hill SC, Coleman M, Beresnev LA, Santarpia JL. Appl Phys Lett 2014;104:113507–10.